UC San Diego
UC San Diego Electronic Theses and Dissertations

Title

Target-Cell-Type Specificity of Corticostriatal Pathways in Movement Control

Permalink

https://escholarship.org/uc/item/994036dk

Author

Lin, Xinlei

Publication Date

2019

Peer reviewed|Thesis/dissertation

UNIVERSITY OF CALIFORNIA SAN DIEGO

Target-Cell-Type Specificity of Corticostriatal Pathways in Movement Control

A Thesis submitted in partial satisfaction of the requirements for the degree Master of Science

in

Biology

by

Xinlei Lin

Committee in charge:

Professor Takaki Komiyama, Chair
Professor Byungkook Lim, Co-Chair
Professor Brenda Bloodgood

2019

The Thesis of Xinlei Lin is approved, and it is acceptable in quality and form
for publication on microfilm and electronically:

_____

_____

Co-Chair

_____

Chair

University of California San Diego

2019

TABLE OF CONTENTS

LIST OF ABBREVIATIONS

CaEvent – Calcium Event

D1 – Dopamine Receptor 1

D1 – Dopamine Receptor 2

DLS – Dorsal Lateral Striatum

GRIN - GRadient INdex

M2 – Secondary Motor Cortex

MSN – Medium Spiny Neurons

PF – Parafascicular Nucleus

PFA – Paraformaldehyde

ROI – Region of Interest

LIST OF FIGURES

ACKNOWLEDGEMENTS

I would like to acknowledge Professor Takaki Komiyama for his support as the chair of my committee. His guidance and valuable suggestions have make significant contributions for my master thesis progression.

I would also like to acknowledge Haixin Liu, who has been critical starting behavioral setup and imaging pipelines for this project. As a mentor, he has taught me many techniques that are essential for experiments. This project would not been possible without his effort.

I would like to acknowledge the Striatum group: Enida Ejoni, Keelin Oneil and Oscar Arroyo. They have been great help for surgeries, histology, imaging and contributing ideas during group meeting. Their contributions were essential for experiment progress.

ABSTRACT OF THE THESIS

Target-Cell-Type Specificity of Corticostriatal Pathways in Movement Control

by

Xinlei Lin

Master of Science in Biology

University of California San Diego, 2019

Professor Takaki Komiyama, Chair
Professor Byungkook Lim, Co-Chair

The striatal direct and indirect pathways exhibit overlapping yet distinct functions in movement planning and control. However, it remains unclear how those distinct functions arise. We investigated an input structure to the striatum, the secondary motor cortex (M2), to find whether this input can potentially drive the functional heterogeneity of direct and indirect pathways in skilled and innate movements. Here, we used monosynaptic retrograde viral labeling, two-

photon imaging and perturbation experiments to investigate the activity correlation between direct/indirect medium spiny neurons (MSNs) in the dorsal lateral striatum (DLS) and their target-cell-type-specific projecting neurons in M2. We found that activity patterns of projecting neurons in M2 do not appear to be overlapping with the activity patterns observed in MSNs in DLS. In addition, perturbations in parafascicular nucleus (PF) led to the abolishment of MSN activities in DLS, while M2 perturbations only decreased MSN activities. Therefore, we proposed that the functional heterogeneity of direct and indirect MSNs in movement control is not likely to be differentiated in M2, and there is a possibility that this heterogeneity can be differentiated in PF.

Introduction

Movement is the essence of life. The ability to make the right movements at the right time is essential for survival. Some movements are innate, such as running away from predators. Some movements require more skills, such as using a fork. In order to make proper movements, both innate and skilled, action planning, execution and cessation are involved. Many areas distributed throughout the brain are important for movements. The motor cortex, basal ganglia and thalamus form an important loop for smooth movement initiation and execution (Shmuelof et al., 2011; Arber et al., 2018). Disruption of the basal ganglia loop is believed to be related to motor diseases including Parkinson's disease (Obeso et al., 2000). As the largest input structure of the basal ganglia, the striatum has been known to be a major integration center that plays a critical role in motor and action planning, motivation, decision-making, reward and reinforcement. Dorsal lateral striatum has been known to be more specifically associated with the motor system (Haber et al., 2000; Haber, 2003; Voorn et al., 2004).

Many studies have investigated the role of direct and indirect pathways of the basal ganglia and their involvement in movement control. Within the striatum, 95% of neurons are medium spiny neurons that send inhibitory inputs to the surrounding nuclei of the basal ganglia (Gerfen, 2004). Striatal MSNs project to the output nuclei of the basal ganglia through direct and indirect pathway projections. MSNs of the direct pathway primarily express the D1 dopamine receptor (D1) and MSNs of the indirect pathway primarily express the D2 dopamine receptor (D2) (Deng et al., 2006; Gerfen et al., 1990). It has been suggested that the direct pathway promotes while the indirect pathway suppresses movements (Freeze et al., 2013; Kravitz et al., 2010). In recent studies, however, there is evidence that a coordinated activity of both direct and

1

indirect pathways is required for movements (Jin et al., 2014; Tecuapetla et al., 2016; Barbera et al., 2016; Klaus et al., 2017).

Taken together, those studies suggest that direct and indirect pathways of the basal ganglia serve overlapping but some distinct functions for motor control. However, the origin of those distinct functionalities remains poorly understood. How do those distinctions of direct and indirect pathways arise? A potential hypothesis is that direct and indirect pathways receive functionally different inputs. Another possibility is that functional distinctions arise in the striatum through local connectivity mechanisms.

Here, we tried to determine the direct and indirect pathway functional heterogeneity in innate and skilled motor behaviors, and we wished to understand if this heterogeneity can be driven by an input region. Therefore, we investigated the correlation between M2 neural activities and DLS neural activities in motor tasks. In additional, we tried to evaluate the contributions of different input structures to DLS including the cortex and the thalamus. Pathway-specific labelling strategy together with two-photon imaging of pathway-specific input neurons was implemented to test the hypothesis that DLS receives functionally distinct inputs from M2. We started with investigating M2 due to its accessibility with cranial windows. If D1 and D2 MSNs can receive functionally segregated information from M2, it is possible that the segregated response patterns of D1 and D2 MSNs are highly correlated with the response patterns of their input neurons in M2.

Methods

All procedures were in accordance with protocols approved by the University of California, San Diego International Animal Care and Use Committee and guidelines of the National Institute of Health. Animals were kept in disposable plastic cages with standard bedding in a room with a reversed light cycle (12 h–12 h). Imaging experiments and perturbation experiments were conducted during night cycle. All animals used in the experiments were Black-6 mice with different genotypes (B6.FVB(Cg)-Tg(Adora2a-cre)KG139Gsat/Mmucd [MMRRC 36158], B6.FVB(Cg)-Tg(Drd1-cre)FK150Gsat/Mmucd [MMRRC 36916], ChAT-IRES-Cre::*frt*-neo-*frt* [JAX006410]).

Pathway-specific labeling strategy:

Transgenic Cre mouse lines were used to achieve pathway specific labeling of MSN projecting neurons. D1R-Cre, A2A-Cre and ChAT-Cre were used for targeting D1 MSNs, D2 MSNs and cholinergic interneurons in the striatum, respectively. Cre-dependent helper virus AAV-DIO-TVA-mRuby and AAV-DIO-RVG, infecting only Cre-positive cells, were used for labeling pathway specific D1-projecting and D2-projecting neurons in M2. AAV helper virus was injected in the dorsal lateral striatum together with implantation of cranial windows. EnvA-mRuby-GCaMP6f was injected three to five weeks followed AAV injection, which allows the expression of GCaMP and mRuby in monosynaptic projecting neurons in different input structures of Cre positive neurons in DLS (Wickersham et al., 2007). Two-photon imaging experiments in M2 were conducted 5 to 9 days after EnvA-mRuby-GCaMP injection.

Surgical Preparation for M2 and DLS imaging:

Surgeries were performed on mice that were 6 weeks older. Isoflurane was used for anesthetizing mice during surgeries. For the implantation of head bars and cranial windows, the scalp was removed, and the skull was scraped following betadine application for preventing infections. After marking the intersection of the midline and coronal suture (bregma), the coordinates of the target area, the dorsal lateral striatum (DLS, 0.5mm anterior, 2.2mm lateral from the bregma, 2.4mm depth from the dura) can be defined with the help of stereotaxic procedures which can help define a plane. A custom head-plate was placed on the skull with superglue followed by dental cement. After the head-plate was fixed, craniotomies were made above DLS to allow AAV helper virus injection with a glass pipette that was front-loaded with the virus. Unilateral injections were made in the right hemisphere of the mouse brain at an injection rate of 20nL per minute. Pipettes were left in the brain for 3 min after injection to prevent backflow. After injection, a chronic cranial window (a glass plug glued onto a larger glass base) was placed on top of M2/RFA (rostral forelimb area).

After three to five weeks of AAV virus injection, 600nL EnvA-mRuby-GCaMP (300nL each, 20mm Z distance away) was injected with the same method into the same coordinates in DLS. The edge of M2 cranial windows were slightly drilled if they were too close to the DLS injection site. After every completion of a surgery, mice were injected with baytril and buprenorphine to prevent infection and swelling and were monitored until they were able to walk around in cages.

For DLS imaging, a Gradient Index (GRIN) lens with 0.5mm diameter was implanted after AAV helper virus injection for deep brain structure imaging. For this, part of the motor cortex needed to be aspirated to allow GRIN lens insertion into DLS. GRIN lenses were kept

approximately at a working distance of 200 microns from the region of interest. After three to five weeks of GRIN lens implantation, *in-vivo* two-photon imaging sessions were performed on those mice.

Behavior Paradigms:

Two behavior paradigms were used to investigate skilled and innate movements. In the ladder paradigm, a wheel-shaped ladder was motorized with repeated sessions consisting of a 1 second auditory cue, 8 second rotating and 6-8 second inter-trial-interval. Mice were head-fixed on top of the ladder to run by grabbing the ladder bars. Therefore, mice were trained to learn how to use forelimbs to grab the bars without falling into the gaps of the ladder. The error rate and limb coordination were improved with 8 days of training. Two seconds before the auditory cue were considered as movement baseline. In the wheel behavior paradigm, a wheel with a continuous plastic surface was used as a platform for mice to run freely on top. In this case, head-fixed awake mice could run and stop voluntarily on top of the wheel, and they were able to run for desired durations. Voltage recoding enables the estimation of the wheel speed. An airpuff pointing towards mouse foot or body was used in order to ensure frequent running. Only 1.5s before and after movement initiation and movement termination were analyzed.

Training:

All three mouse lines (A2A-Cre, D1R-Cre and ChAT-Cre) were trained daily on two rounds of ladder and wheel tasks for four days around 3-4 weeks after AAV injection, specifically 4 days before the EnvA injection. Training was skipped on the injection day. Daily training sessions were resumed the day after EnvA injection for four days. Starting from the fifth

day after EnvA injection, 2-photon imaging sessions were performed in M2 for only five days due to the restriction of EnvA toxicity for neuron health.

Two-photon Imaging:

Imaging was conducted with a commercial two-photon microscope (MOM, Sutter Instrument, retrofitted with a resonant galvanometer-based scanning system from Thorlabs), running Scanimage using a 16× objective (NIKON) with excitation at 940 nm (Ti-Sapphire laser, NewPort) to optimize the visibility of both green (GCaMP6f signal) and red (mRuby signal) channels. For imaging corticostriatal neurons, the objective immersed in double DI water was placed above the cranial window. First, wide field imaging was used to find the brain surface with blood vessels, and then two-photon imaging sessions were performed. In order to investigate as many cortical neurons using two-photon imaging, two fields of view (25 *μm* to 80 *μm* away) were simultaneously acquired at a framerate approximately 14 Hz. Fields with visible neurons were selected randomly ranging from 150 to 650 *μm* depth from the brain surface. Each two-photon imaging session was 25 min long for each task. Head-fixed awake mice were imaged for one task (around 80 trials for ladder or wheel) followed by 80 trials of another task. One-hour resting period was assured for each mouse after one round of imaging session for both tasks. Each mouse was imaged two rounds per day (approximately 100 minute, eight fields in total). Frame times were recorded and Ephus software was used for synchronizing behavioral recordings. After imaging, recorded fields per session were split into two fields.

For imaging striatal D1 and D2 MSNs, the same objective, imaging setup and behavioral setup were applied. Excitation wavelength was set at 925 nm. Two-photon imaging sessions were performed on head-fixed awake mice for one to three days depending on the available fields via GRIN lens. Same dual task imaging strategy described above was used.

Single Cell Activity

Using custom MATLAB program, lateral motion artifacts were corrected by aligning fluorescence images frame by frame (Mitani, 2018) followed by manual regions of interest (ROI) drawing. ROIs marking the cell bodies were drawn by visual inspection based on GCaMP6f fluorescence intensity that was distinguishable from the background at maximal intensity projection. Pixels inside of each ROI ring were considered as a single cell, while pixels extending radially outward from the ROI ring by 6 pixels were considered as background. Pixels were excluded if there were located in overlapping ROI regions. Then, dF/F traces were extracted for each cell and analyzed. Among drawn ROIs, neurons with above-threshold intensity (threshold set at 200 a.u) were used for further analysis. Analyzable neurons were selected if the baseline fluorescent intensity higher than the threshold for both GCaMP and mRuby channels. Neurons with no activity or abnormal activity were excluded from further analysis. The other criteria to select active neurons (a subset of analyzable neurons) was having 2 calcium event transient per minute. Calcium events can be detected if neurons had a fast rising phase, and on average the calcium event duration is 0.5s. Task modulated neurons (a subset of active neurons) were selected using shuffling method (Peters et al, 2014) to detect neurons whose activities were significantly related to the movement period. Task modulated neurons that had activities significantly higher or lower than the movement baseline (2s before the movement onset) were further divided into excitatory and suppressive neurons, respectively. Our analysis excludes neurons that do not show any fluorescence transients during imaging period.

Statistics

In order to characterize neuron's tuning property, each running trial was binned into baseline period (1s to 0.5s before onset), pre-onset period (0.5s to 0s before onset), post-onset

period (1s after onset), pre-offset period (1s before offset), and post-offset period (1s after offset). Activity (dF/F) for each bin was averaged, and each cell had one average dF/F for each bin for all trials. Ranksum test was performed on each cell comparing averaged dF/F of each bin with that of the baseline bin. Then, a cell can be categorized into pre-onset tuned/ post-onset tuned/ pre-offset tuned/ post-offset tuned neurons depending on which bin came out to be statistically different from the baseline bin ($p<0.05$). The percentage of tuned cells were selected from neurons that had at least one calcium event.

In order to define neurons correlated to movement acceleration, each trial was binned at 0.5s. An averaged calcium event and an acceleration can be calculated for each bin. Therefore, correlation coefficient can be calculated for each neuron with all its calcium event values and acceleration values ($p<0.05$).

Muscimol Inactivation:

After all the fields were imaged, muscimol inactivation experiments were performed on a subset of mice implanted with GRIN lens. One of the fields in DLS was selected and imaged with the same two-photon imaging setup for approximately 15 minutes for one task followed by 15 minutes of another task. Muscimol hydrobromide (5 μg/μL, Sigma), a GABAergic agonist, was injected in Parafascicular nucleus or M2 with three volume conditions (25nL, 50nL or 100 Nl). After muscimol injection, a resting period of 30 min to 1 hour was ensured before imaging sessions.

Histology

After imaging sessions or muscimol perturbation experiments, animals were perfused with 4% Paraformaldehyde (PFA) for brain extraction. Extracted brains were stored in PFA for 1-2 days before being transferred to 30% sucrose. Brains sitting in 30% sucrose were ready for

slicing once they sunk to the bottom of the liquid. Brains were cut into 60 or 80 μm slices using a microtome and mounted to glass slides with CC/mount. Some brain slices were stained with GFP primary antibodies and anti-chicken/rabbit secondary antibody before mounting. The staining solutions used were 1:1000 diluted primary/secondary antibody to blocking solution. Blocking solutions were made with 5.4Ml 1X PBS, 60mg 10% BSA, 600μL 10% NGS and 18μL 0.3% Triton 100x. Slices were incubated in blocking solution for 1 hour at room temperature before being transferred to the primary antibody solution overnight at 4°C. Then, slices were washed in PBS 3 times on a rocker for 20 min at room temperature before the 2-hour incubation in the secondary antibody at room temperature. Slices were washed before mounting. Mounted slices were photographed using an Axio-Zoom microscope to visualize viral expression in injection site and projecting neurons in input regions.

Results:

Two-Photon Imaging of MSNs and Its Projecting Neurons in M2

We wished to understand the activity correlation between MSNs and their projecting neurons during motor tasks. Rabies retrograde tracing studies have demonstrated that dorsal striatum receives substantial inputs from the cortex and thalamus (Wall et al., 2013). Among the cortical regions that project to the striatum, M2 has been shown to be significantly active for skilled motor task (Makino et al., 2017). Here, pathway specific labeling strategy (Figure 1A) allows visualization of infected direct or indirect MSN projecting neurons in M2 via cranial windows (Figure 1B). GRIN lens allows imaging of direct or indirect MSNs in DLS (Figure 1C). Dual behavioral tasks allow evaluation of multiple parameters (innate and skilled) for motor tasks (Figure 1D).
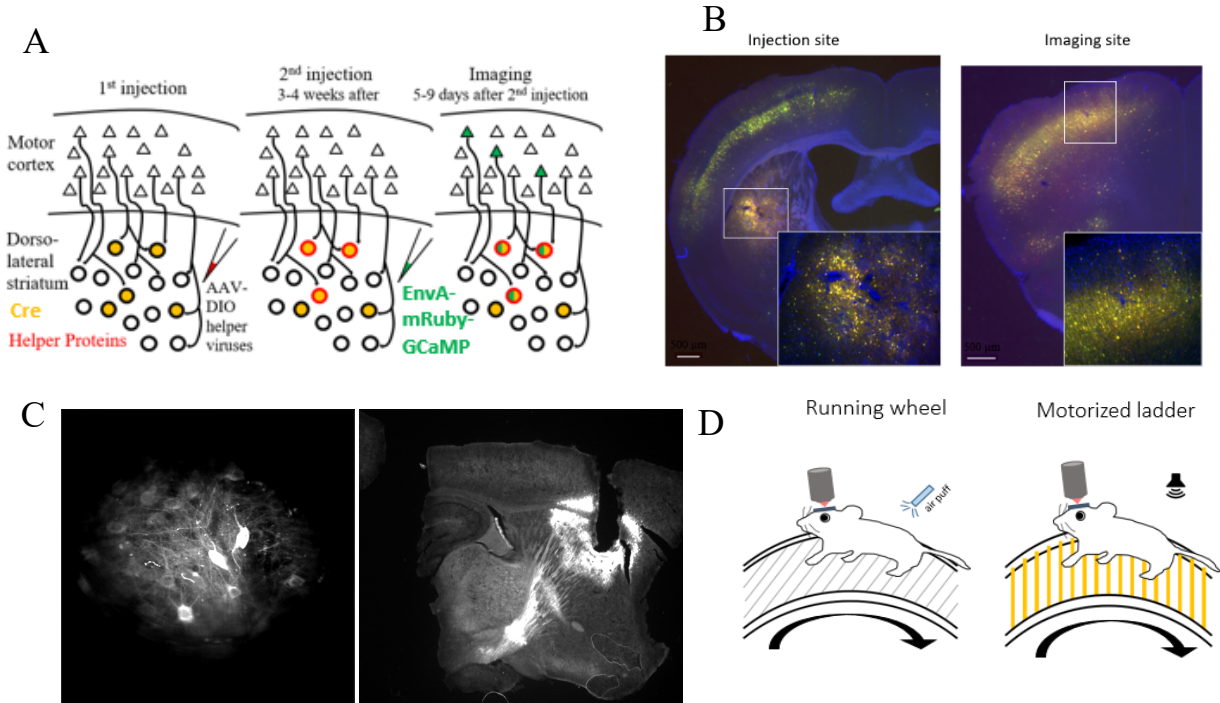
Figure 1: Two-photon calcium imaging of projection neurons in M2 and MSNs in DLS. A) Schematic of pathway specific labeling and injection timeline. B) Histological data from one animal showing injection site in DLS and imaging site in M2. C) Example of two-photon imaging field in DLS through GRIN lens (left); histology showing GRIN lens implantation at DLS(right). D) Schematic of dual behavioral task.
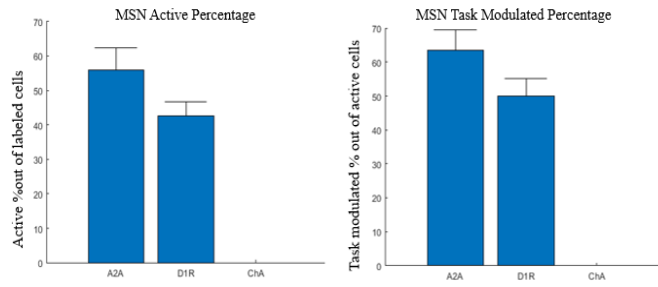
Active Neurons and Task Modulated Neurons

In order to compare neural activity patterns between DLS and M2, the percentage of active neurons, task modulated neurons, excitatory and suppressive neurons in both M2 and DLS were defined and compared across brain regions (Figure 2). The selection of active, modulated, excitatory and suppressive neurons has been described in Method section. In DLS, D1R and A2A MSNs do not differ statistically in the active neuron percentage out of labeled neurons for both tasks or in the modulated percentage out of active neurons using chi square test (Figure 2 A, E). In M2, A2A projecting neurons have higher active percentage than D1R projecting neurons in both innate and skilled tasks (chi square test, $p<0.01$), while having no statistical difference in
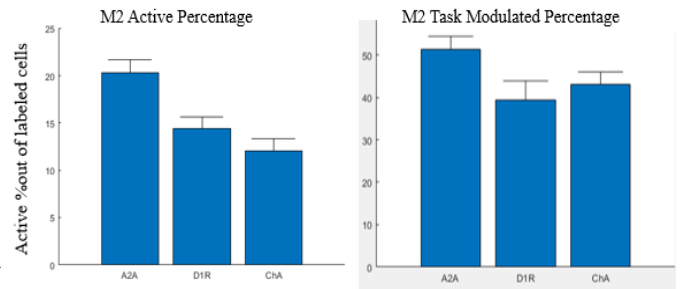
modulated neuron percentage out of active neurons (Figure B, F). Although this could suggest that A2A pathway is unique at the cortex level, the difference in A2A active neuron percentage is very likely due to better surgery yield. As shown in figure 2 (C-D, G-H), the analysis of excitatory response and suppressive response suggests that the major type of response for both MSNs and their projecting neurons was excitatory. In addition, more excitatory responses were also found in A2A MSNs compared to D1R for both innate and skilled tasks (chi square test, $p<0.01$), but the projecting neurons in M2 did not show statistical difference between excitation and suppression for either task (Figure 2C-D, 2G-H). In fact, we found that in M2, A2A-projecting neurons have even slightly higher suppressive response than D1R-projecting neurons for both tasks, which is the opposite of what we found in MSNs (Figure 2 D, H). Since the data from ChA mouse line for cholinergic interneurons in DLS was absent here, and thus only A2A and D1R were compared across brain regions. In summary, for the parameter of active, modulated, excitatory and suppressive neurons, MSNs and their projecting neurons in M2 did not show similarity.

Figure 2: Analysis of active, modulated, excitatory and suppressive neurons. A) Active neuron percentage out of labeled neurons for MSNs in DLS during skilled task (Left). Modulated neuron percentage out of active neurons for MSNs (A2A and D1R) in DLS during skilled task (Right). Note that ChA data is absent in DLS. B) Active neuron percentage out of labeled neurons for MSN-projecting neurons (both A2A and D1R and ChA) during skilled task (Left). Task modulated neuron percentage out of active neurons for MSN-projecting neurons (A2A and D1R and ChA) during skilled task (Right). C-D) Proportion of excitatory neurons (Exc) and suppressive neurons (Inh) out of task modulated neurons during skilled task in DLS and M2. E) Active neuron percentage out of labeled neurons for MSNs in DLS during innate running task (Left). Modulated neuron percentage out of active neurons for MSNs (A2A and D1R) in DLS during innate running task (Right). F) Active neuron percentage out of labeled neurons for MSN-projecting neurons (both A2A and D1R and ChA) during innate running task (Left). Task modulated neuron percentage out of active neurons for MSN-projecting neurons (both A2A and D1R and ChA) during innate running task (Rigt). G-H) Proportion of excitatory neurons (Exc) and suppressive neurons (Inh) out of task modulated neurons during innate task in DLS and M2.
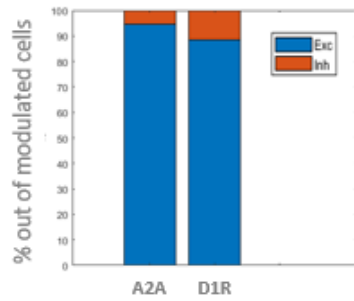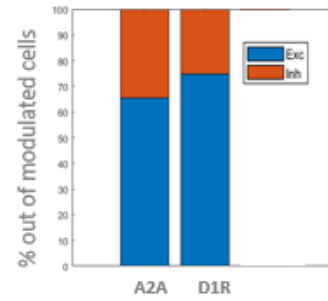
A Skilled Task (DLS)

MSN Active Percentage
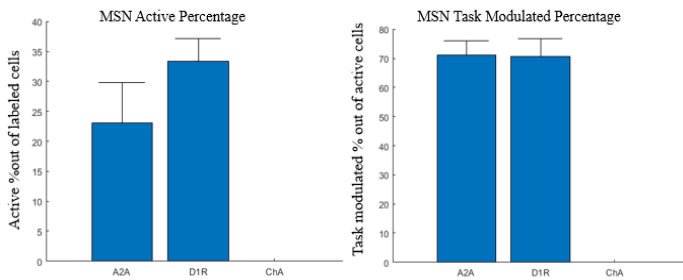
MSN Task Modulated Percentage

B Skilled Task (M2)

M2 Active Percentage

M2 Task Modulated Percentage

C Skilled Task (DLS)

D Skilled Task (M2)

E Innate Task (DLS)

MSN Active Percentage

MSN Task Modulated Percentage

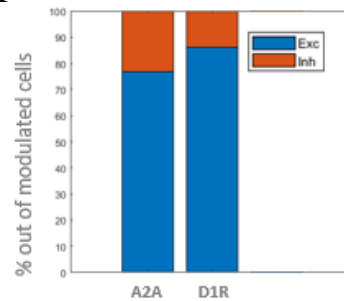**F** Innate Task (M2)

M2 Active Percentage

M2 Task Modulated Percentage
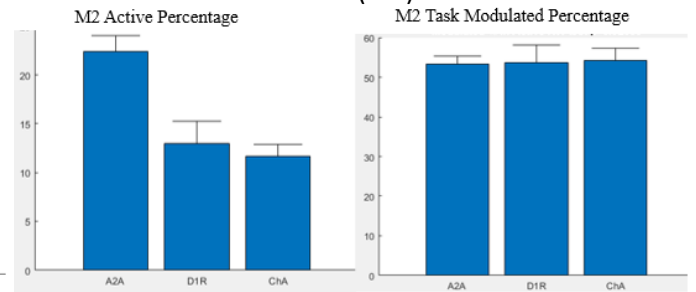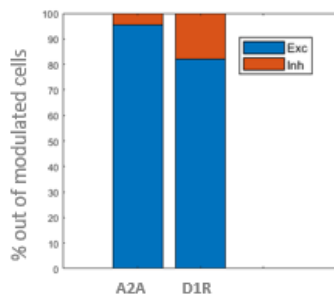
G Innate Task (DLS)

H Innate Task (M2)

A2A and D1R MSNs differ in Population Average Amplitude

We wished to investigate the functional heterogeneity of direct and indirect MSNs and their contributions throughout movement initiation, execution and cessation. Besides, we wanted to know if any correlation related to this parameter can be detected in M2. Population average response can be a useful measure of certain activity kinematics and amplitude patterns. Calcium events averaging all trials for all active neurons during one movement window were plotted for both MSNs and projecting neurons (Figure 3). The auditory cue (cue), movement onset (on) and movement offset (off) have been marked on the plot. A2A MSNs appeared to have higher population response amplitude for both tasks, while the activity kinematics appeared to be quite similar between A2A and D1R. However, in M2, A2A and D1R projecting neurons did not show differential activity amplitude or activity kinematics (Figure 3). Therefore, this result suggests that neurons in M2 and DLS did not exhibit high similarity in population response.
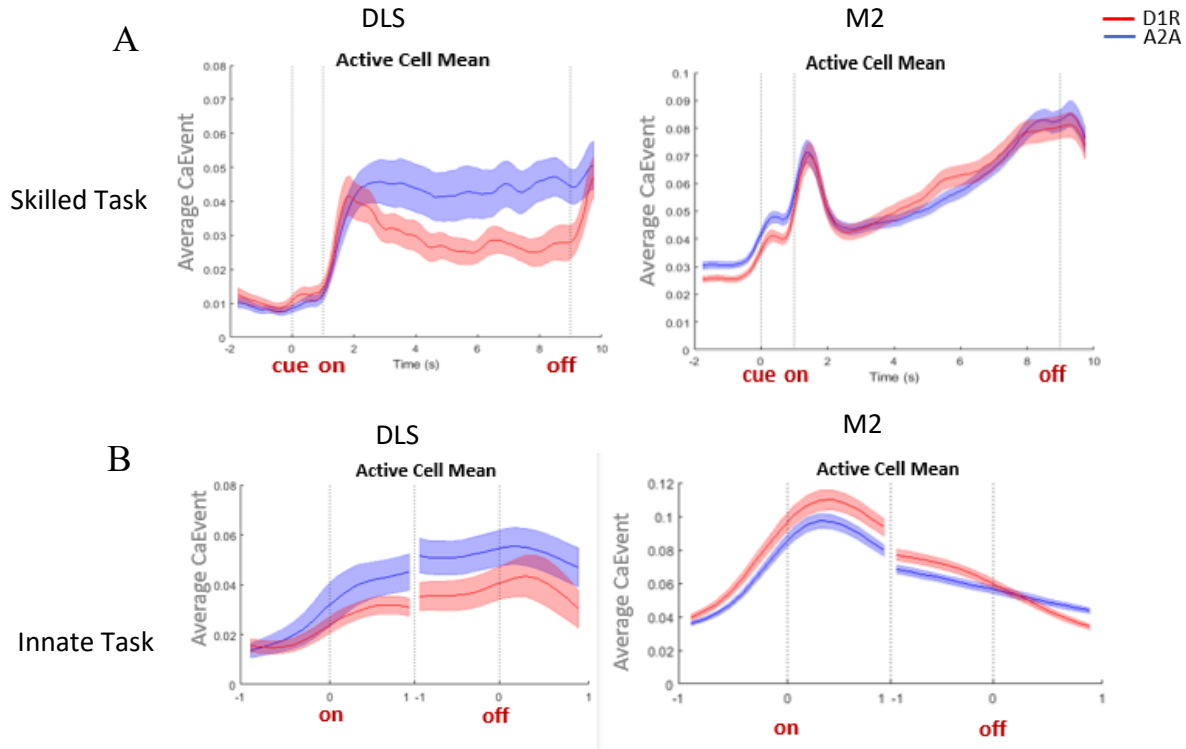
Figure 3: Population response of active neurons. A) Average of calcium event for all active neurons recorded during skilled task in DLS and M2. "Cue" indicates auditory cue; "on" and "off" indicate trial onset and offset. Blue indicates A2A and red indicates D1R. B) Average of calcium events for all active neurons recorded during the innate task in DLS and M2. "On" and "Off" indicate trial onset and offset, and only 1s before and after onset and offset is analyzed for innate running task.

Movement Temporal Tuning

To further investigate the role of neurons in different movement stages, we tried to characterize neurons based on their different temporal contributions throughout the movement window. As described in Method section, we found that neurons can be tuned to a specific time window including movement onset, movement ongoing period and movement offset (Figure 4A). Neurons tuned to those time windows were observed in both M2 and the DLS, in both A2A and D1R neurons and in both innate and skilled movements. Using chi square test for A2A's and D1R's tuning percentages across all bins, we found that more A2A MSNs were tuned to the

movement offset in innate task (p<0.01), but A2A projecting neuron tuning in M2 was not significantly different from D1R projecting neuron tuning in M2 (Figure 4B). In addition, the number of significantly tuned bins was counted for each cell. Among those neurons that show tuning property, A2A MSNs show significantly longer tuning durations than D1R MSNs (higher number of significant bins) in the innate task by chi square test. However, in M2, projecting neurons did not show the similar trend regarding tuning duration. Taken together, the temporal tuning property of MSNs did not share high similarity with projecting neurons in M2.
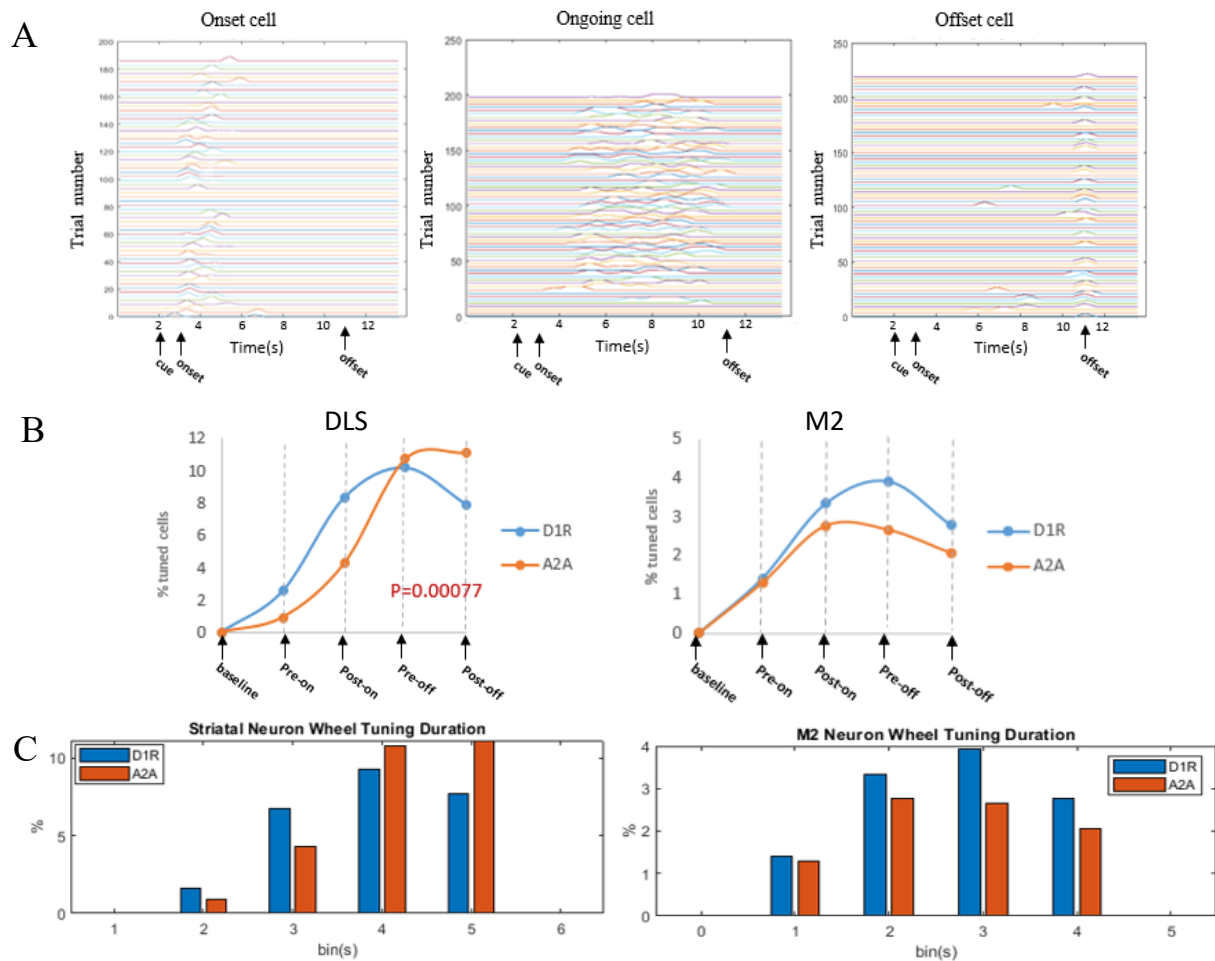

Figure 4: Analysis of cell temporal tuning. A) Example neurons representing neurons tuned to a specific time window during the task including onset tuning (left), ongoing tuning (middle) and offset tuning (right). B) Scattered plot of percentage of neurons tuned to pre-onset, post-onset, pre-offset and post-offset respectively in DLS (left) and M2 (right). C) Bar graph indicating the number of significant bins (x-axis) a neuron had during innate running task. Y-axis indicates the percentage of neurons out of active neurons that had a certain number of significant bins in DLS (left) and M2 (right).

Movement Onset Acceleration Tuning

Acceleration during movement onset is particularly important for a motor task. Acceleration marks the initiation of the movement. We wished to understand if direct and indirect MSNs have differential roles in encoding acceleration during movement onset, and whether their roles in acceleration can be inherited from M2 input. During the innate running task, the wheel voltage recording allowed speed and acceleration calculation. Averaged calcium events for all bins were plotted corresponding to acceleration in Figure 5. By defining acceleration correlated neurons (described in Method) and calculating the percentage of correlated neurons for D1R and A2A neurons, we found that A2A and D1R MSNs exhibit different tuning properties for acceleration during movement onset (Figure 5A). As shown in Figure 5, A2A MSNs show negative correlation ($r = -0.65$, $p < 0.01$) while D1R MSNs showed positive correlation ($r = 0.52$, $p < 0.01$) with onset acceleration. However, in M2, A2A and D1R projecting neurons did not show difference in the signs of correlation, and the two projecting populations are both positively correlated with acceleration during movement onset (Figure 5B). Therefore, we found functional heterogeneity in movement acceleration tuning for MSNs, while this heterogeneity was absent in projecting neurons in M2.
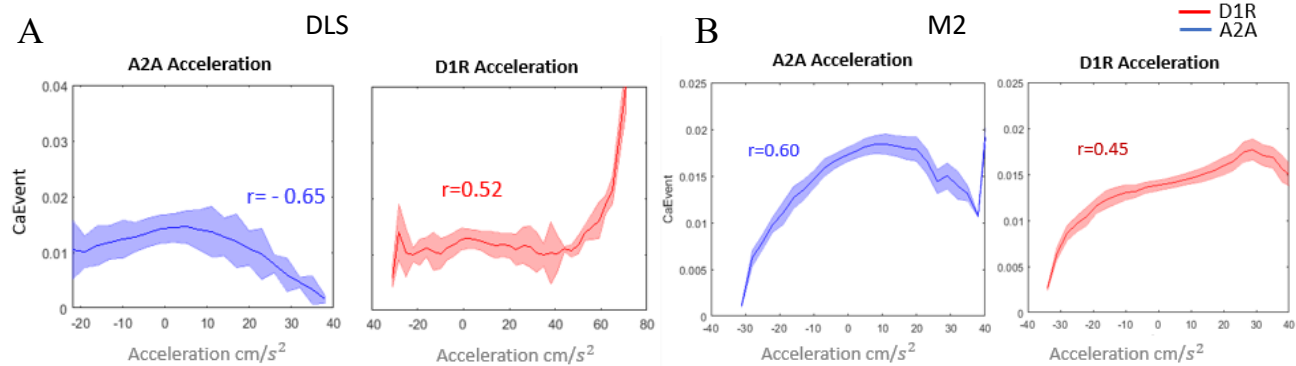
Figure 5: Analysis of cell acceleration tuning. A) The averaged calcium event calculated for each bin with a specific acceleration at movement onset for innate task. X-axis indicates the acceleration in cm/s^2, and y-axis indicates the corresponding calcium event average. A2A and D1R MSNs are plotted in blue and red. B) Same as figure 5A, A2A and D1R projecting neurons in M2 are plotted in blue and red.

Perturbation in PF Abolishes Neural Activity in DLS

Our results above have suggested that neurons in DLS and M2 showed little correlation in many parameters for movements. According to rabies tracing experiments, another major input structure to dorsal striatum is thalamus, and among different thalamic nuclei, parafascicular neucleus gives the largest amount of input to both direct and indirect pathways (Wall et al., 2013). We wished to investigate the function of PF in DLS activity and behavioral output during our motor tasks by perturbation. Strong behavioral phenotype has been observed in mice after PF inactivation. When mice were in the cage after muscimol injection in PF, they showed a hard time executing any simple movements. In the skilled ladder motor task, mice failed to smoothly execute motor commands by putting strong resistance to the ladder and dragging their bodies on the ladder. In innate running task, most mice could barely move on the wheel. In addition, muscimol injection inactivating PF with simultaneous 2-photon imaging DLS showed that MSN activity in DLS was almost abolished during PF inactivation (Figure 6). This dramatic effect

persisted even when the dosage of muscimol and waiting time were halved. Both the neural

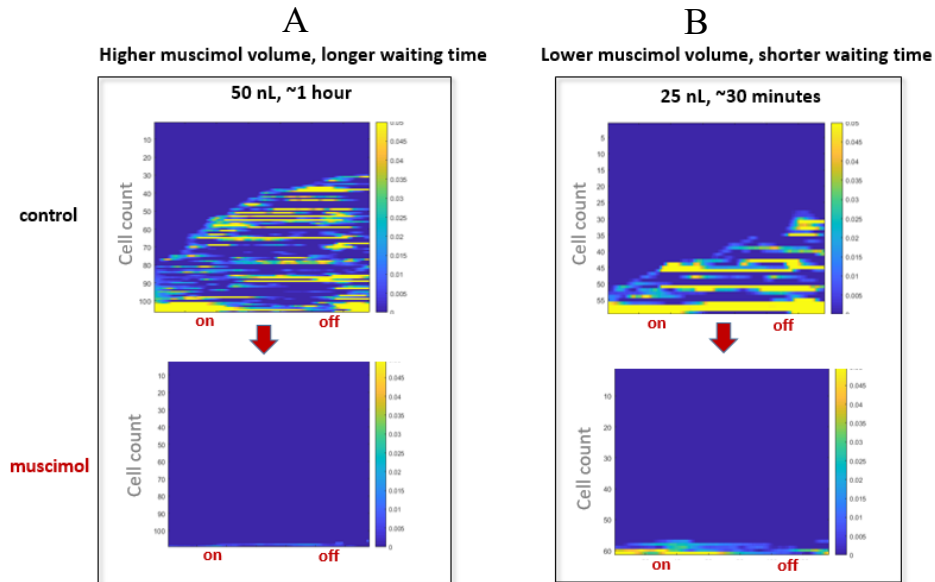activity change and behavioral change were reversible within 24 hours.

Figure 6: Neural activity change due to muscimol perturbation in PF nucleus. A) Averaged dF/F activity for each neuron was plotted as heatmap against the movement window. Movement onset and offset were indicated as "on" and "off". The top indicates the control session and the bottom indicates the muscimol session with 50nL injection volume and 1 hour waiting period before imaging. B) Same as A, but with a lower muscimol injection volume (25nL) and a shorter waiting period (30min).

Perturbation in M2 led to activity decrease in DLS

In order to compare the functional roles of two major input structures to DLS, M2 and

PF, we did the same perturbation experiments in M2. Similar to PF perturbation experiments,

muscimol injection inactivating M2 with simultaneous 2-photon imaging DLS showed that MSN

activity in DLS significantly decreased during M2 inactivation (Figure 7A). However, this effect

was not as robust as PF inactivation. The effect of M2 inactivation did not persist every time

with variation in conditions including halved muscimol volume and waiting time after injection

(Figure 7B). Taken together, many neurons imaged after muscimol in M2 showed major activity

decrease compared to control sessions. However, mice did not exhibit observable phenotype during motor task execution or in the cage. Again, the neural activity changes in DLS were back to normal the next day.

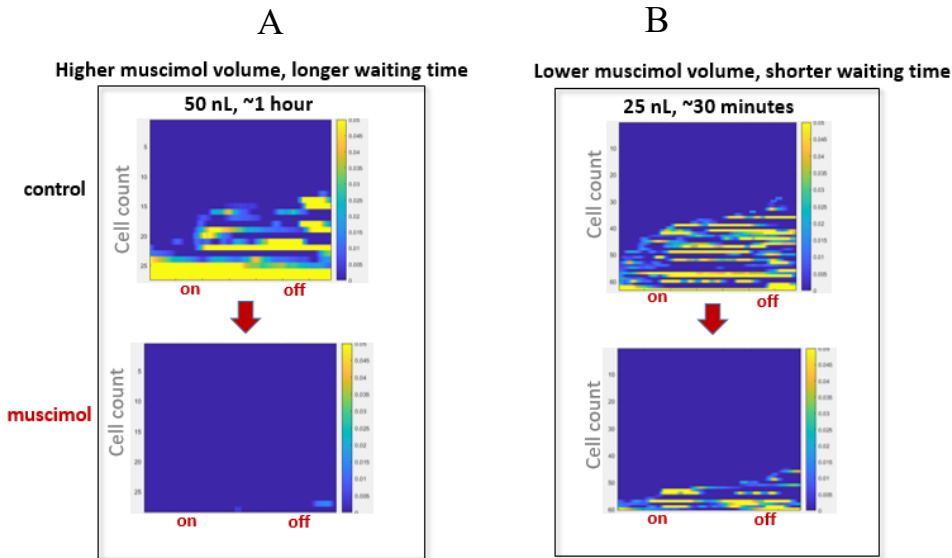A   B

Figure 7: Neural activity change due to muscimol perturbation in M2. A) Averaged dF/F activity for each neuron was plotted as heatmap against the movement window. The top indicates the control session and the bottom indicates the muscimol session with 50nL injection volume and 1 hour waiting period before imaging. B) Same as A, but with a lower muscimol injection volume (25nL) and a shorter waiting period (30min).

Discussion:

Across our data, we found little similarity in activity patterns between MSNs in DLS and projecting neurons in M2 across multiple parameters including active and modulated neurons, excitation and suppression, population response and temporal and acceleration tuning. In general, the functional heterogeneity we found in MSNs were absent in M2. First, A2A MSNs exhibit higher excitatory response than D1R MSNs for both motor tasks, while this difference was absent in A2A and D1R projecting neurons in M2. A2A MSNs also showed higher activity amplitude of population response, even though the kinematics during movement shared more

20

similarities. This is more consistent with the hypothesis that the co-activation of D1 and D2 MSNs was required for movement execution. Again, unlike MSNs, the population response for D1 and D2 projecting neurons in M2 during the movement were highly similar both in kinematics and amplitude. In addition, D1 and D2 MSNs showed different acceleration and temporal tuning, but projecting neurons in M2 did not exhibit corresponding differences. Although it remains unclear how much overlap exists between the cortical projections to D1 and D2 MSNs, the high similarity between D1 and D2 projecting neurons in M2 can potentially suggests that the percentage of cortical neurons projecting to both D1 and D2 MSNs can potentially be high. The only similarity that was shared between striatal and cortical neurons was the higher A2A active percentage out of labeled neurons in skilled task. However, this can due to better surgery yield instead of the actual activity correlation. The low correlation between MSNs and projecting neurons in M2 indicates that M2 is probably not the information segregation source for D1 and D2 MSN activity during movement control. This is based on the assumption that highly correlated cell populations are generally connected via strong synaptic projections (Cossell et al., 2015).

Perturbation experiments in M2 and PF can tell us more about the functional role of those input regions. Related to the previous point, the fact that M2 inactivation did not lead to consistent and robust abolishment of MSN activity in DLS may suggest that the connections from M2 might not be required for driving DLS activity. However, the fact that there is at least a decrease in M2 inactivation indicate that M2 might be important for certain aspects of the movement encoding. Besides, M2 inactivation seems to cause a much milder behavioral phenotype compared to PF inactivation. The difference in inactivation effect between M2 and PF can suggest different mechanisms of how different inputs can regulate the same region. For

21

example, PF can project to the whole DLS, while M2 only projects to a smaller portion of DLS, which allows for compensating mechanisms when M2 is inactivated. The different levels of severity between M2 and PF inactivation not only suggest different mechanisms for regulating downstream targets, but also indicate the possibility that thalamic inputs may serve to drive the functional differences in direct and indirect pathways. In summary, the functional differences in D1 and D2 MSNs do not seem to arise from the secondary motor cortex. The question of whether PF and DLS can be correlated still needs to be investigated.

Conclusion:

Our data suggested that the direct and indirect pathways in the basal ganglia shared some overlapping while distinct features for our motor tasks. However, the activity patterns of MSNs in DLS did not overlap with their projecting neurons in M2. Our perturbation experiment results have shown stronger effects of PF inactivation on MSN activity in DLS, which could suggest that instead of M2, a plausible region that gives functionally distinct inputs to the DLS during motor control can be PF.

References:

1) Haber, SN. (2003). The primate basal ganglia: parallel and integrative networks. Journal of Chemical Neuroanatomy, 26(4):317-30.

2) Harber SN., Fudge, JL., McFarland, NR. (2000). Striatonigrostriatal pathways in primates form an ascending spiral from the shell to the dorsolateral striatum. *The Journal of Neuroscience*, 15;20(6):2369-82.

3) Voorn, P., Vanderschuren, LJ., Groenewegen, HJ., Robbins, TW., Pennartz, CM. (2004). Putting a spin on the dorsal-ventral divide of the striatum. *Trends in Neuroscience*, 27(8):468-74.

4) Obeso, JA., Rodriguez-Oroz, M., Rodriguez, M., Lanciego, J., Artieda, J., Gonzalo, N., Olanow, W. (2000). Pathophysiology of the basal ganglia in Parkinson's disease. *Trends in Neuroscience*, 23(10 Suppl):S8-19.

5) Deng, YP., Lei, WL., Reiner, A. (2006). Differential perikaryal localization in rats of D1 and D2 dopamine receptors on striatal projection neuron types identified by retrograde labeling. *J Chem Neuroanat*, 32:101–116.

6) Gerfen, CR., Engber, TM., Mahan, LC., Susel, Z., Chase, TN., Monsma, FJ., Sibley, DR. (1990). D1 and D2 dopamine receptor-regulated gene expression of striatonigral and striatopallidal neurons. *Science*, 250:1429–1432

7) Gerfen, CR. Basal Ganglia. In: Paxinos G, editor. The Rat Nervous System (Third Edition) Burlington: Academic Press; 2004. pp. 455–508

8) Peters, A.J., Chen, S.X. and Komiyama, T. (2014). Emergence of Reproducible Spatiotemporal Activity During Motor Learning. *Nature,* 510(7504), 263-7. doi: 10.1038/nature13235

9) Makino, H.*, Ren, C.*, Liu, H.*, Kim, A.N., Kondapaneni, N., Liu, X., Kuzum, D. and Komiyama, T. (2017). Transformation of cortex-wide emergent properties during motor learning. *Neuron*, 94(4), 880-90.

10) Benjamin, S. Freeze., Alexxai, V. Kravitz., Nora, Hammack., Joshua, D. Berke., and Anatol, C. Kreitzer. (2013). Control of Basal Ganglia Output by Direct and Indirect Pathway Projection Neurons. *Journal of Neuroscience*, 33(47), 18531–18539.

11) Kravitz, AV., Freeze, BS., Parker, PR., Kay, K., Thwin, MT., Deisseroth, K., Kreitzer, AC. (2010). Regulation of Parkinsonian Motor Behaviours by Optogenetic Control of Basal Ganglia Circuitry. *Nature,* 466(7306):622-6.

12) Jin, X.*, Tecuapetla, F., and Costa, R.* (2014). Basal Ganglia Subcircuits Distinctively Encode the Parsing and Concatenation of Action Sequences. *Nature Neuroscience*, 17(3), 423–430.

13) Tecuapetla, F., Jin, X., Lima, SQ., Costa RM. (2016). Complementary Contributions of Striatal Projection Pathways to Action Initiation and Execution. *Cell,* 166(3):703-715.

14) Hyun Joo Lee, Andrew J. Weitz, David Bernal-Casas, Ben A. Duffy, ManKin Choy, Alexxai V. Kravitz, Anatol C. Kreitzer, and Jin Hyung Lee. (2016). Activation of direct and indirect pathway medium spiny neurons drives distinct brain-wide responses. *Neuron*, 91(2): 412–424.

15) Klaus, A., Martins, GJ., Paixao, VB., Zhou, P., Paninski, L., Costa, RM. (2017). The Spatiotemporal Organization of the Striatum Encodes Action Space. *Neuron*, 95(5):1171-1180.e7.

16) Barbera G, Liang B, Zhang L, Gerfen CR, Culurciello E, Chen R, Li Y, Lin DT. (2016). Spatially Compact Neural Clusters in the Dorsal Striatum Encode Locomotion Relevant Information. *Neuron*, 92(1):202-213.

17) Wall NR, De La Parra M, Callaway EM, Kreitzer AC. (2013). Differential Innervation of Direct- and Indirect-Pathway Striatal Projection Neurons. *Neuron*, 79(2):347-60.

18) Mitani, A. and Komiyama, T. (2018) Real-Time Processing of Two-Photon Calcium Imaging Data Including Lateral Motion Artifact Correction. *Frontiers in Neuroinformatics*, doi:10.3389/fninf.2018.0009

19) Shmuelof, L., Krakauer, JW. Are we ready for a natural history of motor learning? (2011). *Neuron*, Nov 3;72(3):469–476.

20) Arber, S. and Costa RM. Connecting neuronal circuits for movement. (2018). *Science*, Jun 29;360(6396):1403–1404.

21) Wickersham, IR., Lyon, LC., Barnard, R., Mori, T., Finke, S., Conzelmann, K., Young, J., Callaway, EM. (2007). Monosynaptic Restriction of Transsynaptic Tracing from Single, Genetically Targeted Neurons. *Neuron,* 53(5):639-647.

22) Cossell, L., Iacaruso, MF., Muir. DR., Houlton, R., Sader, EN., Ko, H., Hofer, SB., Mrsic-Flogel, TD. (2015). Functional Organization of Synaptic Strength in Primary Visual Cortex. Nature, 518(7539):399-403